J. Am. Soc. Mass Spectrom. (2016) 27:1772–1786
DOI: 10.1007/s13361-016-1458-1

CRITICAL INSIGHT

Distance-of-Flight Mass Spectrometry: What, Why, and How?

Elise A. Dennis,[1,5] Alexander W. Gundlach-Graham,[1,4] Steven J. Ray,[2] Christie G. Enke,[3] Gary M. Hieftje[1]

[1]Department of Chemistry, Indiana University, Bloomington, IN 47405, USA
[2]Department of Chemistry, State University of New York at Buffalo, Buffalo, NY 14260, USA
[3]Department of Chemistry and Chemical Biology, University of New Mexico, Albuquerque, NM 87131, USA
[4]*Present Address:* Department of Chemistry and Applied Biosciences, ETH Zurich, 8093, Zurich, Switzerland
[5]*Present Address:* Perkin Elmer, Shelton, CT 06484, USA

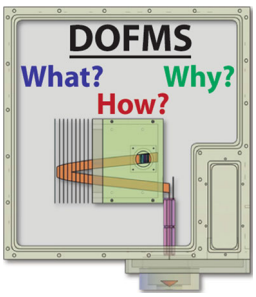

Abstract. Distance-of-flight mass spectrometry (DOFMS) separates ions of different mass-to-charge (*m*/*z*) by the distance they travel in a given time after acceleration. Like time-of-flight mass spectrometry (TOFMS), separation and mass assignment are based on ion velocity. However, DOFMS is not a variant of TOFMS; different methods of ion focusing and detection are used. In DOFMS, ions are driven orthogonally, at the detection time, onto an array of detectors parallel to the flight path. Through the independent detection of each *m*/*z*, DOFMS can provide both wider dynamic range and increased throughput for *m*/*z* of interest compared with conventional TOFMS. The iso-mass focusing and detection of ions is achieved by constant-momentum acceleration (CMA) and a linear-field ion mirror. Improved energy focus (including turn-around) is achieved in DOFMS, but the initial spatial dispersion of ions remains unchanged upon detection. Therefore, the point-source nature of surface ionization techniques could put them at an advantage for DOFMS. To date, three types of position-sensitive detectors have been used for DOFMS: a microchannel plate with a phosphorescent screen, a focal plane camera, and an IonCCD array; advances in detector technology will likely improve DOFMS figures-of-merit. In addition, the combination of CMA with TOF detection has provided improved resolution and duty factor over a narrow *m*/*z* range (compared with conventional, single-pass TOFMS). The unique characteristics of DOFMS can enable the intact collection of large biomolecules, clusters, and organisms. DOFMS might also play a key role in achieving the long-sought goal of simultaneous MS/MS.

Keywords: Distance-of-flight, Time-of-flight, Sector field mass spectrometry, IonCCD, Inductively coupled plasma, Matrix-assisted laser-desorption ionization, MALDI

Received: 20 January 2016/Revised: 15 July 2016/Accepted: 19 July 2016/Published Online: 25 August 2016

Introduction and Perspective

Mass spectrometers are now ubiquitous in analytical laboratories, and the range of applications, environments, and measurements to which mass spectrometry (MS) is applied is extensive. An impressive but not comprehensive list of research fields outside analytical chemistry influenced by MS development includes forensics [1, 2], archaeology [3], physics [4], cosmology [5–7], geosciences [8], atmospheric sciences [9, 10], materials science [11], biosciences [12, 13], and medicine [14]. Moreover, the analytical performance of modern mass spectrometers is compelling. For example, state-of-the-art ion-cyclotron resonance (ICR) mass spectrometers can routinely discriminate between species that are separated by only 0.001 *m*/*z*; this resolution is sufficient to discriminate between isobaric chemical species and to provide empirical chemical formulas directly [15]. Modern sector-field mass spectrometers, in combination with the inductively coupled plasma (ICP) ionization source, can measure a wide range of ion fluxes, from <10 to 10^{12} counts per second, and deliver extremely low detection limits (<10 pg/L) [16]. Time-of-flight (TOF) mass spectrometers can deliver entire mass-spectra at rates of thousands per second, which is often necessary for transient analyses [17].

Unfortunately, the state-of-the-art performance characteristics identified above are neither available on a single MS platform nor best suited for all MS applications. No mass

Correspondence to: Gary M. Hieftje; *e-mail:* hieftje@indiana.edu

spectrometer design is (or probably can be) ideal for all MS applications. Just as the scope of MS applications is broad, so are the types of mass spectrometers. If we consider just mass analyzers—not in combination with the numerous varieties of ion sources or in connection with separations methods or in combination in MS/MS instruments—we are still left with a long list (acronyms in order of invention): TOFMS[1] [18], SFMS[2] [19], FTICR-MS[3] [20, 21], Q-MS[4] [22, 23], QIT-MS[5] [22, 23], QqQ-MS[6] [24–27], Orbitrap [28], and DOFMS[7] [29]. Consequently, the question of what distinguishes one mass-analysis approach from another is pivotal and non-trivial; in this regard, many authors have attempted to define and categorize mass analyzers according to performance characteristics and basis of operation [17, 30–32]. Here, we seek to identify where DOFMS fits within the landscape of mass-analyzer designs (cf. Figure 1) and to provide insight into how developments in DOFMS instrumentation and theory could impact MS analysis. To accomplish these tasks, we emphasize how DOFMS compares with other MS methods in terms of the mode of mass separation and performance characteristics, highlight some of our most critical results, and then, based on the knowledge we have gained, provide an outlook for future advances in DOFMS and potential applications.

Description of DOFMS

DOFMS features analytical performance characteristics similar to those of both TOFMS and multichannel SFMS. As a velocity-based approach (analogous to TOFMS), DOFMS has the potential to provide high-speed spectral generation, full-spectrum generation, high (10%–100%) duty-cycle data collection, and has a theoretically unlimited mass range. DOFMS also has a simple instrument design that requires only electrostatic components. As a spatially dispersive technique (akin to multichannel SFMS), DOFMS benefits from the measurement of ion flux across space, which allows the use of a charge-based detector array that could offer greater precision and dynamic range than is available with high-speed TOFMS detectors.

Like in TOFMS analyzers, in DOFMS, ion packets are accelerated to *m*/*z*-dependent velocities, and these velocities are measured to determine an ion's *m*/*z*. But there are two ways to measure velocity. One method is to measure the time required for ions to go a certain distance (e.g., TOFMS). The other is to measure the distance traveled in a given time. Time-of-flight MS uses the first approach, whereas distance-of-flight MS uses the second. In a similar vein, both approaches are used in chromatography: in column chromatography we measure *when* compounds elute (retention time), and in thin-layer chromatography we measure how *far* molecules travel. Figure 2 depicts a type of spatially dispersive SFMS known as a Mattauch-Herzog geometry mass spectrograph (MHMS), an orthogonal-acceleration reflectron TOFMS system, and a DOFMS instrument for a direct comparison of the techniques.

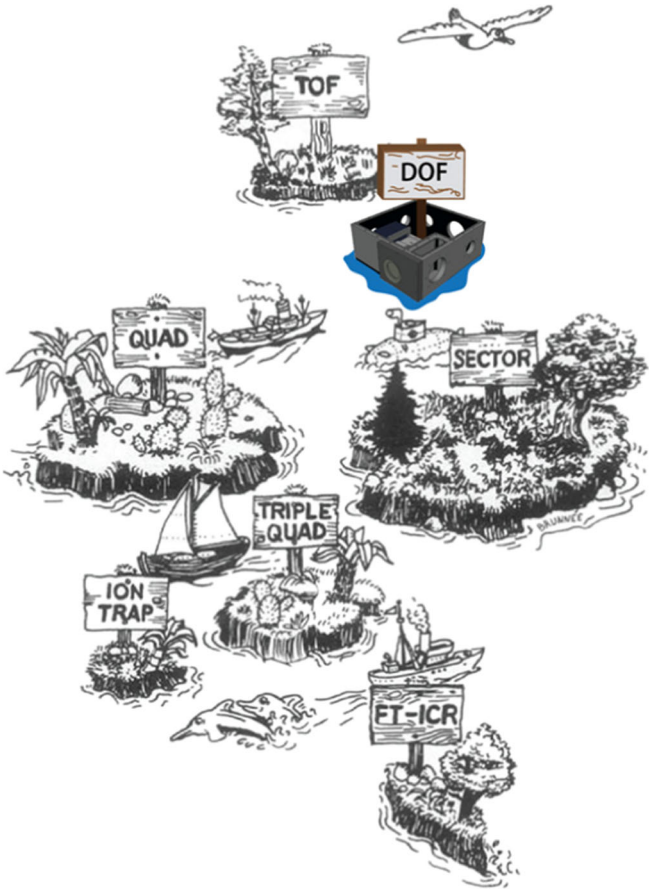

Figure 1. In 1987, Kurt Brunée imagined the "mass-spectrometer islands" in a cartoon representation of the distinction among mass analyzers based on analyzer-specific performance characteristics [31]. Although Brunée's analysis is dated, it is still pertinent: no MS instrument satisfies all user requirements. Importantly, Brunée's MS islands indicate that there is room for bridging MS technologies. Here, we have inserted the island of DOFMS in the channel between SFMS and TOFMS because DOFMS combines attributes of both approaches; namely, DOFMS is a velocity-based *m*/*z* separation like TOFMS and a spatially dispersive *m*/*z* separation similar to SFMS. The DOFMS island is illustrated as the CAD image of the first DOFMS vacuum chamber instrument, though in reality it certainly wouldn't float

As Figure 2 highlights, there are clear similarities between DOFMS and both TOFMS and MHMS. DOFMS and TOFMS have very similar instrumental layouts (i.e., a field-free region, a reflectron, etc.); however, disparate from TOFMS, which utilizes constant-energy acceleration, DOFMS requires a constant-momentum acceleration (CMA) pulse, a linear-field reflectron, and a spatially selective detection system. This spatially selective detector can be identical to those found in MHMS instruments as shown in Figure 2. Just as in other spatially dispersive MS approaches, such as the MHMS, in

[1]Time-of-flight mass spectrometry (TOFMS)
[2]Sector-field mass spectrometry (SFMS)
[3]Fourier transform ion cyclotron resonance mass spectrometry (FTICR-MS)
[4]Quadrupole mass spectrometry (Q-MS)
[5]Quadrupole-ion trap mass spectrometry (QIT-MS)
[6]Triple quadrupole mass spectrometry (QqQ-MS)
[7]Distance-of-flight mass spectrometry (DOFMS)

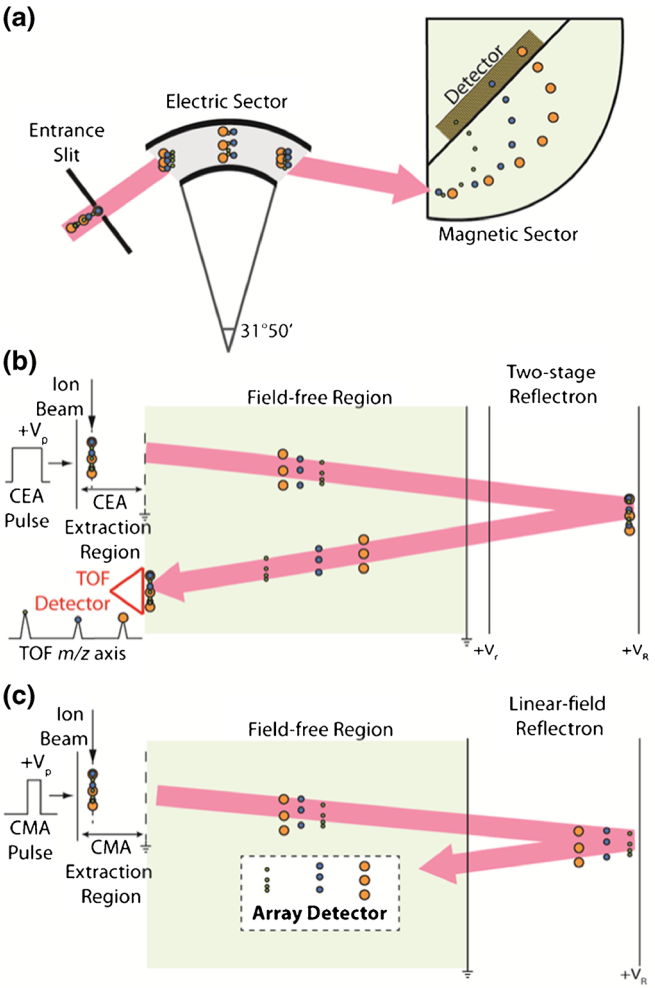

Figure 2. Diagrams of (**a**) a Mattauch-Herzog geometry mass spectrograph (MHMS), (**b**) an orthogonal-acceleration TOFMS instrument, and (**c**) a DOFMS instrument. The flight path of ions through each instrument is emphasized. The mass spectrograph and DOFMS share physical separation of the masses and the same type of detection, but the pulsed extraction, velocity separation, and reflectron aspects are shared between DOFMS and TOFMS. These diagrams are not drawn to scale, but are meant to illustrate the similarities and differences between mass separation in DOFMS and the more conventional TOFMS and MHMS systems

DOFMS, when ions strike the detector, their impact position along the mass-separation axis is related to *m*/*z*. So, even though DOFMS separation accelerates packets of ions and the MHMS disperses a steady stream of ions, the same detectors can be used.

Table 1 outlines the major differences between DOFMS and other common mass-analysis techniques. Among the various mechanisms used to distinguish ions of different *m*/*z*, only TOFMS and DOFMS employ ion velocity. Also, they both use a reflectron for ion focus, but the nature of the achieved focus is different. The remainder of this paper will detail these distinctions, while pointing out where the special characteristics of DOFMS can be used to particular advantage.

Comparison of TOFMS and DOFMS

One of the major obstacles in the development of TOFMS was achieving adequate ion focusing to realize meaningful results. The TOFMS ion-focusing problem arises because ions do not all start at the same position (spatial dispersion) or with the same kinetic energy along the TOF separation axis (energy dispersion). As a result, ions of the same *m*/*z* value do not have identical velocities in the flight tube and will not arrive at the detector at the same time if their velocity spread due to space and/or energy distributions is not compensated. Because of these limitations, the resolution of the first TOFMS instruments was so poor that they were easily displaced by early, relatively crude quadrupole analyzers.

With modern temperature-controlled electronics, clever pulsing schemes, and ion-beam collimation techniques, TOFMS is among the highest-resolution analyzers available. For the interested reader, a recent review of ion-focusing improvements was published by Radionova et al. [33]. Since the initial realization of TOFMS, the incorporation multi-stage extraction and acceleration, the orthogonal acceleration geometry, and the reflectron into TOFMS instrument designs have significantly improved performance. The reflectron mirrors the space-focus plane onto the TOFMS detector and, thereby, extends the length of mass separation and helps compensate for energy dispersion. Introducing ions with orthogonal acceleration reduces both energy and spatial dispersion along the mass-separation axis. Both an orthogonal-acceleration region (or planar ion source) and a reflectron are used in DOFMS in order to operate optimally. However, the consequences from the use of each of these techniques differ for DOFMS and TOFMS, as the modes of ion acceleration and ion focusing are dissimilar.

In order to appreciate fully how and why DOFMS is distinct, particularly from TOFMS, it is necessary to understand the fundamental differences between constant-energy and constant-momentum acceleration [34].

Acceleration of ions to a constant energy for TOFMS is achieved by application of an electrostatic field over a known distance (from an ion's initial position to the exit of the acceleration region). By this method, all ions starting from that point, regardless of *m*/*z*, are sent into the mass-separation region (the flight tube) with the same nominal boost in energy. Variations in initial ion position (spatial dispersion) result in different ion velocities after acceleration that are partly compensated at the space-focus plane of the acceleration region. *Initial* ion-energy disparities (energy dispersion) also result in ion-velocity differences after acceleration. These initial-energy-based disparities are partially corrected by the reflectron but cannot be perfectly compensated. The turnaround time that results from acceleration of rearward-moving ions causes unavoidable peak broadening [35] and is often the major source of peak width; in TOFMS analyzers, turnaround-time error can be

Table 1. Common Mass Analyzers and Some of Their Defining Characteristics

Analyzer	Ion separation property/ mechanism	Packet/ Stream	Detector type	Spatially dispersive? Y/N	Focusing	Limitation on upper mass
Magnetic sector	Momentum	S	Single	N	Slit	Magnetic field, acceleration voltage stability
Electric sector	Kinetic energy	S	Single	N	Slit	None
Focusing mag. sect.	Momentum	S	Array	Y	Slit	Magnetic field, acceleration voltage stability
Double- focusing	Energy and momentum	S	Single	Y	Slit	Magnetic field, acceleration voltage stability
Linear quadrupole	Trapping stability	S	Single	N	None[a]	Detector, applied waveform characteristics
Quadrupole ion trap	Secular frequency	P	Single	N	Collisional	Detector, applied waveform characteristics
FTMS, Orbitrap	Secular frequency	P	Induction	N	Duration of frequency measurement	Detector, applied waveform characteristics
Time-of-flight	Velocity	P	Single	N	Reflectron	Detector
Distance- of-flight	Velocity	P	Array	Y	Reflectron	Detector

[a]When utilized as a stand-alone mass spectrometer.

minimized only by using delayed or high-field extractions, which makes the turnaround as quick as possible [15].

By contrast, in the case of constant-momentum acceleration (CMA), employed for DOFMS, ions in the acceleration region gather speed across a constant field-strength for a specified time and, therefore, receive the same change in nominal momentum, regardless of m/z [36]. However, having the same momentum but different masses gives them m/z-dependent energies. Since no ions of interest exit the region during the brief CMA pulse, there is no measurable effect of an ion's initial position on the outcome of acceleration. Instead, the original width of the ion packet is preserved during ion flight in the field-free region. In other words, there is no space-focus plane: the initial spatial distribution of ions is neither focused nor defocused after CMA and is exactly the same at the position of detection as in the acceleration region. This behavior favors, of course, a very narrow or focused input ion beam or ions originating from a planar surface. In CMA, an ion's initial energy does, however, add to (or subtract from) its final velocity after acceleration. In DOFMS, this energy-dependent velocity difference is compensated in the linear-field reflectron, which energy-focuses ions at their m/z-dependent flight distances at a particular time called the energy focus time (t_{ef}). In DOFMS, all ions are detected at this single t_{ef} in order to provide best resolution. Importantly, at t_{ef} both initially forward- and reverse-moving ions are focused, which means there is no turnaround-time error. This error ultimately limits resolution in conventional TOFMS [37], although ion cooling, trapping, ion-beam shaping, and high extraction fields help to minimize turnaround-time errors. The key mathematical relationships that describe energy-focusing CMA operation have been described in detail elsewhere [29, 34, 38–40].

A prototype DOFMS instrument has been constructed and used to test the principles of DOFMS [40]. The mass analyzer consists of a set of dc quadrupole ion optics to focus the input ion beam into an orthogonal-acceleration region, followed by an approximately 30-cm field-free flight zone and a linear-field reflectron. Along the flight path, and after the reflectron, a second acceleration region is used to orthogonally push m/z-separated ions onto a spatially selective detector. To date, several detection systems have been tested with the prototype system—they will be discussed in detail shortly. Initial experiments with DOFMS have been conducted with atomic ionization sources including a reduced-pressure direct-current glow discharge [39, 41–43] and an inductively coupled plasma [44–46].

To further illustrate the significance of ion-focusing principles in DOFMS, Figure 3 displays results from a computer simulation (SIMION) of ion trajectories in our DOFMS instrument. In this experiment, two initial starting conditions for ions in the acceleration region are tested: in Figure 3a, ions are started with no initial energy along the mass-separation axis, but are spread uniformly across 4 mm of the acceleration region (along the mass-separation axis). In Figure 3b, ions are started with no initial spatial spread, but a convergent focus produces an energy distribution of ±0.02 eV. These two sets of ions were then subjected to identical DOFMS conditions and the widths of the ion packets along the mass-separation axis were computed. As seen in Figure 3c, the width of the initially collimated ion packets at the DOFMS detector are exactly the same as when they began because no spatial focus is achieved for DOFMS. Similarly, the ion packet that started with a distribution of energies but no spatial spread also delivers ions onto the DOFMS detector with conserved initial spatial distribution. Overall, the mass resolution available in DOFMS is dictated almost entirely by the width of the initial ion beam and the length of the field-free flight region; for a m/z-independent initial beam size, the mass resolution in DOFMS is constant across all mass ranges. It follows that a narrowly focused ion beam is ideal for CMA (in combination with a reflectron) because the spatial width of the ion beam is minimized and the velocity vectors are focused at t_{ef}. Interestingly, the convergent ion focus best suited for DOFMS is opposite that of orthogonal-acceleration TOFMS, which provides optimal

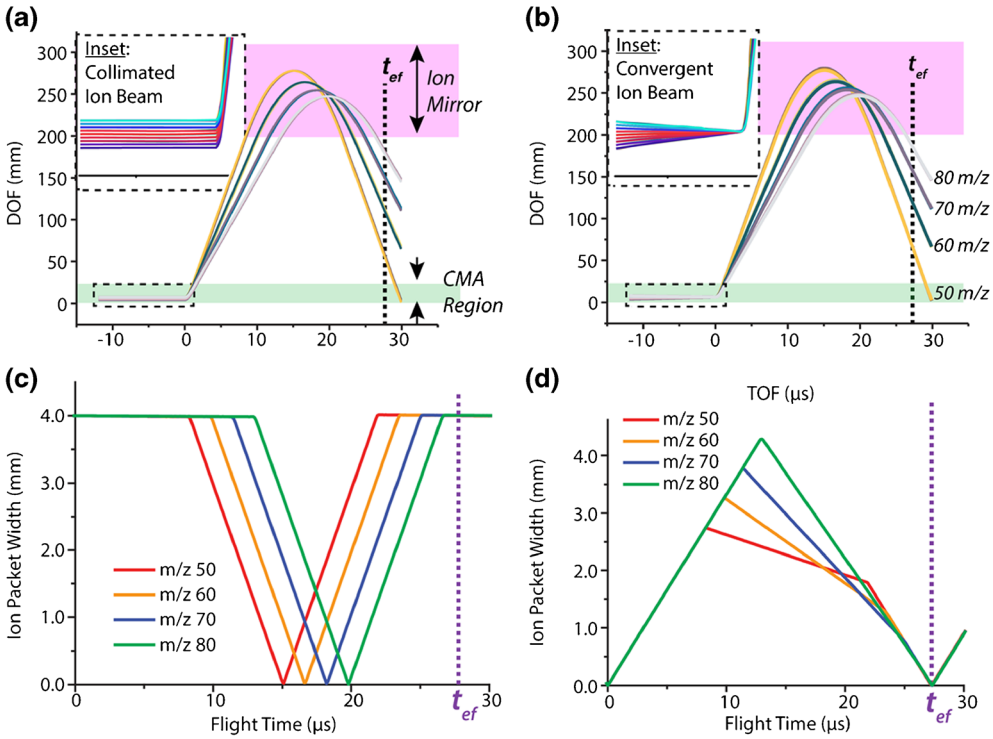

Figure 3. Results from a SIMION simulation of ion trajectories in a virtual DOFMS instrument. In the simulation, ions are accelerated to a constant momentum at time zero, fly through a field-free region, turn around in a linear reflectron, and should be detected at an energy-focus time (t_{ef}) of 27.5 µs. Two initial ion populations are considered: one with a 4-mm uniform width across the acceleration region (**a**), and one with no spatial distribution, but an energy distribution caused by convergent-beam focusing (**b**). As seen in (**c**) and (**d**), the DOFMS instrument reproduces the ion-packet width at t_{ef} that existed at the start of CMA extraction for all ions across the DOF mass-separation axis. At t_{ef}, the DOFMS instrument compensates for initial energy distributions, but provides no focusing for initial spatial distributions

performance if the initial ion beam is collimated in the first stage of the acceleration region [37, 47]. Apart from providing improved resolution for DOFMS, the CMA-based ion-focusing scheme used in DOFMS can be exploited in TOFMS. Recently, we have developed a new zoom-TOFMS scheme, which can be used to eliminate the effects of turn-around time-error in TOFMS and, over a narrow m/z range, provide better mass resolution and higher ion throughput than conventional TOFMS [48]. Zoom-TOFMS will be described later.

Equation 1 relates ion flight distance to m/z for DOFMS and shows how the flight distance at the energy-focus time is—to a first approximation—directly related to initial ion position, but independent of initial ion energies, which is apparent in Figure 3. At the energy focus time (t_{ef}), the first term gives the nominal distance of flight. In Equation 1, q_e is the charge on an electron, s_0 is the average initial ion position, Δs_0 is the distance from s_0 of the ion's initial position, U_0 is the initial ion kinetic energy, (E_P) is the electric-field strength in the acceleration region, (τ) is the duration of the CMA pulse, and (E_M) is the constant electric field within the reflectron. From Equation 1 we see that the distance at t_{ef} is inversely proportional to m/z. The second term gives the spatial dispersion of the ions at detection and confirms that it is the same as the ions had at the time of acceleration. The last term reflects a second-order energy factor that is uncorrected—dispersion caused by this term will be proportional to the initial ion kinetic energy.

$$L_{FF}@t_{ef} = \frac{zq_eE_P}{m}\left(\frac{2E_P\tau}{E_M} - \frac{\tau}{2}\right) - (s_0 + \Delta s_0) - \frac{4|U_0|}{zq_eE_M} \quad (1)$$

$$t_{ef} = \frac{4E_P\tau}{E_M} \quad (2)$$

Figure 4 demonstrates the effect of t_{ef} on the DOFMS mass spectrum of $^{107}Ag^+$ and $^{109}Ag^+$ measured with a MCP-phosphor detection assembly and CCD camera. In this experiment, the duration (τ) of the CMA pulse was changed, but nothing else. A change in τ alters the momentum received by ions and thus changes t_{ef} as shown by Equation 2. For any particular imparted momentum ($mv = zq_eE_P\tau$), there exists only one t_{ef} at which ions of all m/z values are energy-focused at m/z-specific positions along the DOF flight path. In Figure 4, the silver isotopes arrive at the MCP detector in focus only if τ is between 3.9 and 4 µs; however, by simple adjustment of electrostatic potentials in the DOFMS

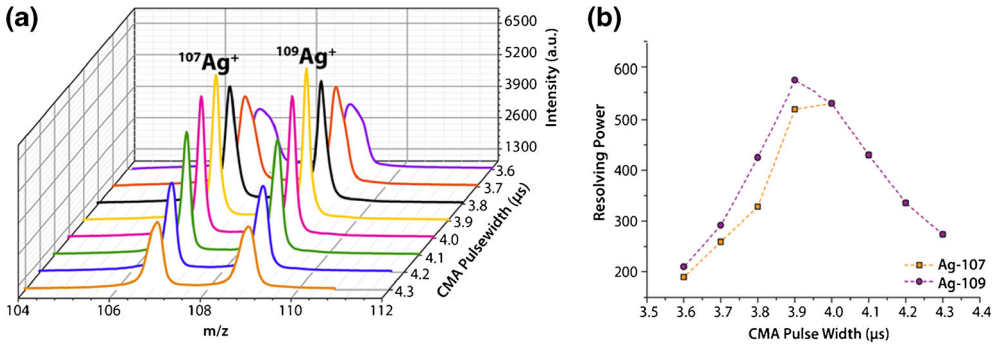

Figure 4. (**a**) Mass-calibrated DOFMS spectra were recorded with a series of increasing CMA pulse durations, from 3.6 to 4.4 µs, whereas all other instrument parameters remained constant. Only with the correct momentum imparted (i.e., with the correct τ value) are the silver isotopes detected in focus across the DOFMS detector. Ions of all other *m/z* are also in focus at t_{ef}; they simply are not at positions to strike the detector. (**b**) Effect of CMA pulse duration on resolving power (FWHM). Improvement in resolution is clear when ions are detected at t_{ef}

instrument, ions of any *m/z* value can be brought onto any detector position at the optimal t_{ef}.

Detector Requirements and Opportunities in DOFMS

Since ions of differing *m/z* are physically separated in DOFMS and because flight distance is used to determine each *m/z*, a spatially selective ion-detection system is required. The performance of the DOFMS detector will, in large part, dictate instrument capabilities; therefore, the identification and development of detector technologies is pivotal to the future of DOFMS. The ideal detection system would have an arbitrarily large number of individual detection elements (i.e., pixels), have a broad dynamic range, have no mass bias, and have quick readout times. The detector array should also be as long as practical to cover the widest possible mass window in each DOFMS spectrum. The span of this mass window depends upon instrument parameters as shown in Equation 3,

$$\frac{\left(\frac{m}{z}\right)_{HIGH}}{\left(\frac{m}{z}\right)_{LOW}} = \frac{L_D}{L_{FF(HIGH)} + S_0} + 1 \qquad (3)$$

where $(m/z)_{LOW}$ is the lower bound of the mass range and $(m/z)_{HIGH}$ is the upper limit of the mass range, $L_{FF(HIGH)}$ is the field-free (flight tube) length to the near side (high-mass side) of the DOFMS detector, s_0 is the distance ions travel in the acceleration region, and L_D is the detector length. Other constraints on the geometry of the DOFMS exist [29], but are beyond the scope of this overview.

In our 27-cm flight-length prototype DOFMS instrument described earlier, for example, a detector 1-inch (2.54 cm) in length will cover a mass range of 6.4 u at $m/z = 100$, but 64 u at $m/z = 1000$. Conveniently, the *m/z* dependence on distance means that the ratio of upper and lower *m/z* values remains constant, so the range of the mass window increases linearly with *m/z*. The spatial resolution of the detector is a major factor in determining the best spectral resolution that the instrument can achieve. As described previously, DOFMS makes use of primary ion-beam focusing to limit the initial spatial distribution of the ions; because that initial spatial width is mirrored on the detector surface, the mass resolution of DOFMS is strongly affected by the fidelity of the ion optics. In turn, this means that the spatial resolution required of the ion detector might depend upon the intended application. As a benchmark, for applications with a mass range around 4000 *m/z* and the same instrument geometry, a detector resolution of approximately 10 µm would be necessary to place 10 resolution elements across a peak; such a peak would be of similar width to that observed with sector-field mass spectrometers. Of course, these detector requirements will likely change as new applications are defined.

Let us contrast DOFMS detection with that of TOFMS. In TOFMS, a single detector is used, TOFMS peaks are temporally very narrow, and the detector time response directly affects mass resolution. In addition, dynamic range is often compromised to avoid detector saturation and consequently slow recovery. In contrast, DOFMS allows analog detection and continuous integration to be used because each *m/z* resolution element is at a discrete location. Not only does this capability expand dynamic range, it also enables better ratio precision to be achieved for a given integration time just by use of less dilute samples. Of course, continuous integration is not the only operational mode for DOFMS—short integration times (100–150 ms) have been utilized to record data for transient laser-ablation events [43]. The ability to handle higher ion throughput will also improve quantitation in molecular analyses, perhaps competing with the quadrupole mass filter [42, 48].

Since temporal response is not directly linked to mass resolution in DOFMS, alternative detection schemes can be explored. For example, direct ion-charge integration, which is not practicable with TOFMS, is quite readily employed in DOFMS. Detection strategies that exploit secondary electron multiplication, such as microchannel plates (MCP), are well known to suffer from gain suppression due to saturation and to show a significant loss of sensitivity [49–51]. In contrast, direct ion-charge detection provides a signal that is directly

proportional to ion charge and has no mass bias, so large biomolecules can be detected as easily as electrons, and positive and negative ions can be registered directly and with equal sensitivity [52]. Finally, the physical separation of ions promises alternative approaches to simultaneous detection and collection of the ions. For example, a soft-landing probe could be incorporated into a DOFMS instrument for nondestructive ion or targeted isotope collection. These mass-separated, collected ions could then be further characterized with techniques such as surface-enhanced Raman spectroscopy or electron microscopy, which have already been demonstrated with soft-landing mass spectrometry [53, 54].

Three position-sensitive ion detectors have been tested in our prototype DOFMS instrument [39, 41, 45] and the two that have been thoroughly evaluated are summarized in Figure 5. The readily available commercially and less expensive choice is the electro-optic ion detector (EOID) [55], comprised of a set of MCPs coupled to a phosphor screen (cf. Figure 5a). As ions strike the MCP, electrons are amplified and exit the stacked MCP pair to strike the phosphor screen, resulting in a luminescent image that can be collected with a CCD camera and quantified [44]. The second detector, the focal-plane camera (FPC) [56, 57], is the integrating semiconductor-based array of charge detectors shown in Figure 5b.

A substantial benefit of the EOID detector is that MCPs and phosphor screens can be made to almost any form factor. As illustrated by Figure 5a, the ion beam is taller than it is wide at the detection plane and the ability of the EOID system to integrate a large portion of the peak height can increase sensitivity. However, because a MCP detector is used to amplify all ions within the window, a common gain setting must be used and can limit the available dynamic range in a particular run. In practical application, a loss of mass resolution is also often observed because of spatial spreading of the electron image by Coulombic repulsion. Another limitation of the MCP-based detector is that mass range is limited because the kinetic energy of large biomolecular ions, for example, is converted largely into internal energy when the ion strikes the MCP surface.

A better approach for DOFMS detection is the use of semiconductor-based mass-spectrometry detectors. Here, fabrication strategies from the semiconductor industry can be leveraged in order to create high-performance detector arrays

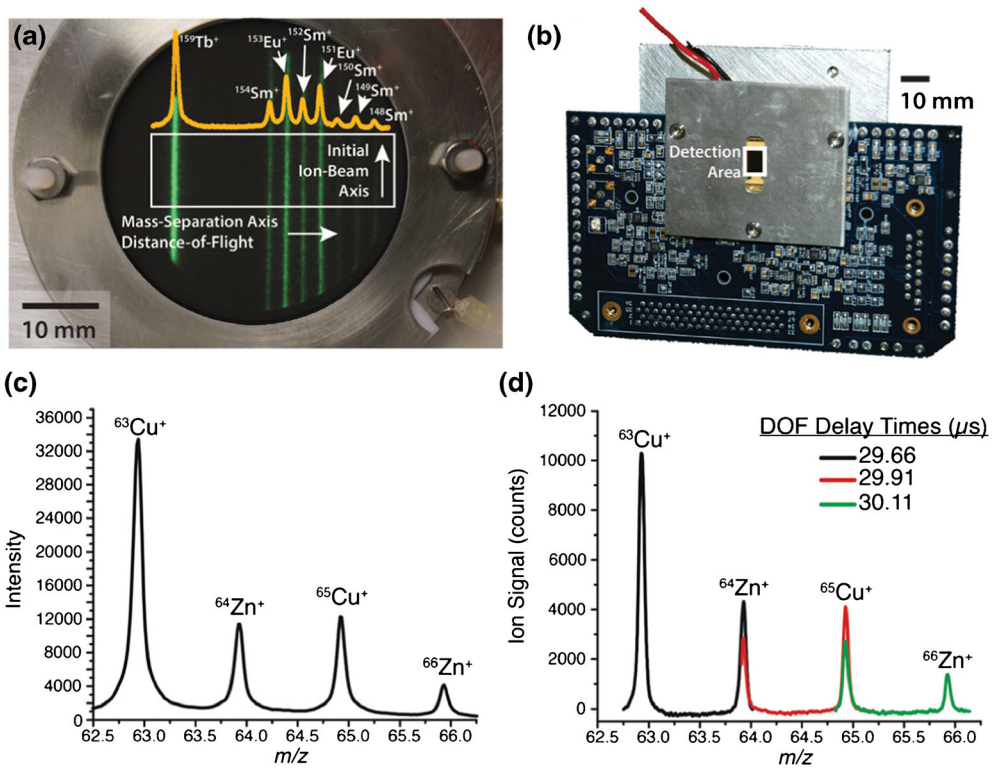

Figure 5. (**a**) Top-down view of the MCP-phosphor detector. DOFMS signals appear as green vertical lines on the image, where the height of each line is due to the section of the initial ion beam sampled with each CMA extraction event. Increasing distance of flight runs from left to right (high to low *m/z*) and the relative intensity of each DOFMS line corresponds to the isotopic abundance of each detected nuclide. To generate a mass spectrum, image pixels are vertically summed along the initial ion-beam axis, within the white box. (**b**) Image of the focal-plane camera detector with 512 discrete charge-integrating detectors (i.e. the FPC-512). (**c**) Mass-calibrated DOFMS spectrum of the copper and zinc isotopes obtained with a 25-mm diameter MCP detector (reprinted from [39]). (**d**) Mass-calibrated spectrum obtained with the FPC-512 detector array. Because the FPC has an active detection length of only 6.4 mm, the mass spectrum of the copper and zinc isotopes had to be acquired in three separate DOFMS experiments. In general, we have found that the FPC provides about twice the resolving power than the MCP/phosphor because it detects ions directly without resolution-worsening effects of secondary-electron amplification

capable of very sensitive position-referenced ion-charge integration. A comprehensive review of these detectors can be found elsewhere [58, 59]. One example, the Focal-Plane Camera (FPC), has been tested with DOFMS and is depicted in Figure 5b [41]. The FPC is comprised of a 1-D array of ion-collection electrodes termed Faraday strips, each of which is connected to a dedicated integrating amplifier circuit [56–58, 60–62]. The amplification circuitry is fabricated monolithically in silicon as a charge-integrating operational amplifier. As ions strike the Faraday strips, charge is integrated onto the feedback capacitor and converted to a proportional voltage by the operational amplifier integrator circuit. The charge-to-voltage gain has two levels achieved by switching between two capacitors. Semiconductor fabrication allows the feedback capacitance to be very low (~8 fF), so high gains are possible (~20 μV/fundamental charge), and detection limits competitive with those of conventional analog ion detectors can be obtained (~20–50 fundamental charges) [57]. Further, the ability to computer-control the detection array offers significant benefits. For example, each ion-detection element can be fabricated with a number of computer-switchable gain settings and can be interrogated individually, with the gain being changed on-the-fly depending on the ion flux striking the element. Each detection element can also be read out repeatedly in a nondestructive manner, minimizing read noise and allowing each element to be queried at a rate dictated by the measurement requirements.

Characterization of DOFMS with a commercially available IonCCD camera (courtesy of O.I. Analytical) is currently underway [45]. Being based on semiconductor array-detection technology, the IonCCD camera detector provides many of the same features as the FPC; namely, the IonCCD camera suffers no mass bias (i.e., it directly detects ion charge), has isolated charge-detection surfaces, and boasts nondestructive readout. In addition, the IonCCD camera is considerably larger than the FPC at 5.1 cm in length (compared with only 0.64 cm for the 512-pixel FPC tested with DOFMS). This extra detection span enables a much larger portion of the mass spectrum to be measured at once.

A mass spectrum that spans most of the atomic mass range (*m*/*z* 57–229) has been collected with the IonCCD detection system and is shown in reference [45]. That mass spectrum was obtained by combining 11 individual spectra that spanned the *m*/*z* 57–229 range; each of these 11 spectra represents 100 averaged collection runs, each taken with a 500 ms integration time. Because the instrument is currently operated manually and instrument parameters must be adjusted between successive mass-spectral ranges, an estimate of total "laboratory time" for the *m*/*z* 57–229 is not available [45]. However, if the adjustment time between runs is neglected, the total acquisition time for the full spectrum is just less than 10 min, with each spectral window requiring about 50 s. A mass spectrum for the isotopes of Europium obtained with the IonCCD camera detector is shown in Figure 6.

Unlike in TOFMS, mass-spectral acquisition time in DOFMS is highly dependent on the type of detector that is utilized. Each of the three detectors discussed here (EOID, FPC, and IonCCD) has a different integration and readout time for DOFMS. The EOID is limited by the CCD camera that is used to capture light from the phosphor screen. For the CCD camera (iKon CCD; Andor Technologies plc., UK) coupled to the DOFMS system for LA-ICP-DOFMS [46], typical exposure times were 100–150 ms, and CCD readout times for single-pulse LA acquisition (CCD was binned 4 × 4) were 0.09025 s. As a result, the CCD was integrating ion signal for 52%–63% of laboratory time [46]. In the case of the FPC, the limiting factor is not the camera electronics but the software in place to read out the camera—LabVIEW. The readout rate of the setup is, therefore, limited to 1 kHz, but this rate is not a function of the DOFMS experiment itself [45]. A brief discussion of ion-collection time with the IonCCD camera is provided above. Since the noise floor (or signal needed to generate a count) on the IonCCD camera is at least an order of magnitude higher than that of either the EOID or FPC, longer integration times (≥500 ms) were necessary to generate comparable signal-to-noise performance [45]. Also, the detection readout speed of the IonCCD camera is limited to ≤360 Hz [45]. Obviously, for all three detectors, at a sufficiently short integration time there will not be enough ion signal for peaks to be observed. The integration time at which the signal level is below detectable range is dependent not only on the detection and ion-focusing systems but also on the ionization source.

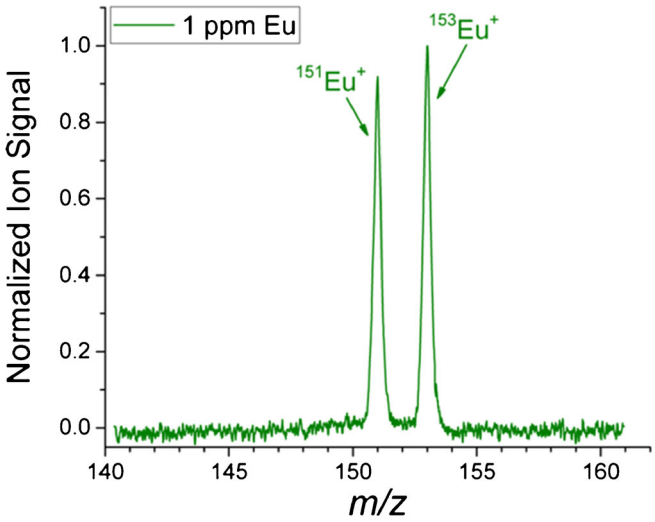

Figure 6. The mass-calibrated spectrum shown here was obtained with the IonCCD detector and an inductively coupled plasma ionization source. The spectrum shown is an average of 50 individual mass spectra each collected with 500 ms integration times

In summary, DOFMS is a high-repetition rate batch technique like TOFMS, but it uses ion travel distance as the means of *m*/*z* separation, an array of independent ion detectors, and focuses initial energy dispersion rather than spatial dispersion. In some respects, DOFMS more closely resembles the MHMS, except DOFMS uses a pulsed ion source and resolution does not depend on throughput-limiting ion slits. The commercial development of DOFMS clearly will depend on the evolution of solid-state ion detector arrays.

To date, DOFMS has been implemented with atomic ion sources that produce very hot ions. The beam formed from these high kinetic-energy ions suffers significant axial and radial dispersion, and appreciable defocusing from the second-order dispersion term in Equation 1. Even so, the proof-of-principle instrument platform designed, built, and tested at Indiana University has demonstrated the significant advantages that DOFMS can bring to elemental and isotope ratio analysis [39, 41–46]. Based on this work, it is reasonable to anticipate that a molecular-analysis version of this instrument, employing the ion cooling and focusing techniques commonly used with atmospheric molecular-ion sources, will yield still better sensitivity and resolution.

New Opportunities

Each new form of mass analyzer has expanded the range and impact of mass spectrometry, not just by providing better performance for existing applications and modes of operation but by opening new areas of application. That evolution has been true for each new breakthrough and it seems likely DOFMS will be no exception. In the following sections, we outline potential (some already demonstrated) new areas that can take advantage of the unique combination of characteristics that DOFMS offers.

Zoom-TOFMS

Zoom-time-of-flight mass spectrometry (zoom-TOFMS) is a technique related to DOFMS that has recently been developed as a low-cost complementary mode of operation for existing or custom-designed TOFMS instrumentation [48]. Stated simply, zoom-TOFMS is a combination approach that switches between conventional CEA-TOFMS and energy-focusing CMA-TOFMS. In CEA-TOFMS mode, the TOFMS instrument operates as a conventional TOFMS instrument. The system can then be switched to CMA-TOFMS "zoom" mode to interrogate a relatively narrow, selectable mass region with improved resolution and duty factor. This zoom mode operates identically to DOFMS, except a stationary TOFMS detector is used along the flight path instead of the spatially dispersive detector. In zoom mode, a target mass window is detected at t_{ef} by the TOF detector, which can be thought of as a single pixel in a DOFMS array detector. Since only ions detected at (or near) t_{ef} are energy-focused, only a narrow region of m/z-values can be interrogated with the zoom mode. In fact, the zoom mode is much like the operation of a zoom lens on a camera—you see a smaller region with greater clarity.

Zoom-TOFMS is capable of resolution improvements in CMA mode for a few reasons. First, the energy focus generated at t_{ef} for CMA is accompanied by a maintained (and controllably narrow) spatial distribution of ions from acceleration region to detector, which together produces narrower mass-spectral peaks than the space-focus provided by CEA [34]. Second, the relationship between m/z and TOF is linear for CMA-TOFMS, whereas the same relationship is square-root-dependent in CEA-TOFMS [38]. This difference in temporal mass spacing leads to increased distance between peaks (especially at high masses) and, therefore, improved mass resolution. The last reason for narrower peaks is the absence of turnaround-time errors from the orthogonal-acceleration process, which has already been discussed for DOFMS.

An existing, heavily modified commercial R.M. Jordan instrument was retrofitted with an extended orthogonal-acceleration region and a linear-field reflectron for initial zoom-TOFMS studies. With this instrument, we [48] demonstrated that zoom-mode operation provides up to a 1.7-fold improvement in mass resolution over CEA-TOFMS, while also enabling the ion-packet introduction rate to be increased up to 100 kHz in zoom mode for an m/z-window at least 12 mass units wide [48]. Increased repetition rates in zoom mode are possible because ions have m/z-dependent energies and, therefore, the target mass range can be isolated by means of kinetic-energy filtering [48].

Since our 2014 publication [48], the field-free region of the zoom-TOFMS instrument has been extended from 0.43 m to 1 m; results are shown in Table 2. A reduced-pressure, direct-current glow discharge (dcGD) ionization source was operated in a 0.5 Torr argon atmosphere (>9% purity, Airgas Inc., Radner, PA, USA) to collect the results reported in Table 2; the sample was a solid block of non-standardized copper. The general operating characteristics for the zoom-TOFMS prototype with the dcGD are identical here to those described previously [48]. The results in Table 2 show a 1.3× average improvement in resolving power (full-width at half-maximum, RP_{FWHM}) for zoom mode compared with CEA-TOFMS mode.

Table 2. Mass Resolution for Both the CEA- and CMA-TOFMS Operational Modes of a 1-m Zoom-TOFMS Instrument. Reduced-Pressure Glow-Discharge Ion Source with Copper Cathode

Element	CEA-TOFMS		CMA-TOFMS	
	RP_{FWHM}	Peak Width (ns, FWHM)	RP_{FWHM}	Peak Width (ns, FWHM)
Cu	3100	5.7	3900	4.7
Sn	3000	7.8	4300	6.1
Pb	3000	10.4	3800	8.7
Average	3030	8.0	4000	6.5

RP_{FWHM} = resolving power at FWHM.

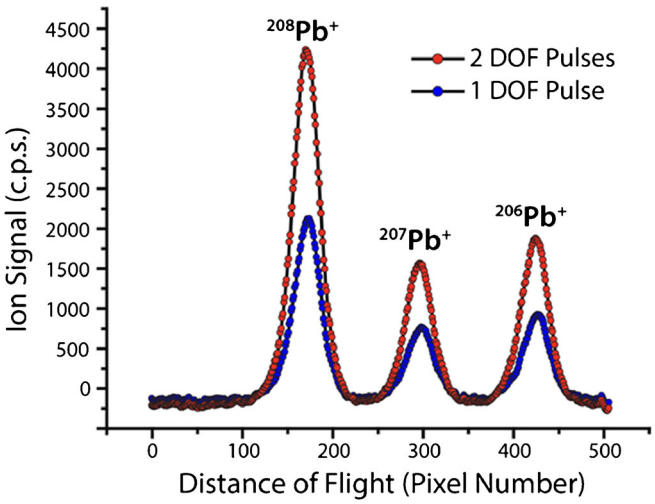

Figure 7. Mass spectra acquired without (blue) and with (red) the interleaved DOFMS approach demonstrate the signal enhancement that can be achieved

The enhanced mass resolution in zoom mode is accompanied by improved sensitivity (from the enhanced duty factor) [48]. In contrast, multi-turn and multi-pass TOFMS instruments can greatly improve mass resolution, but they do so at the expense of spectral-generation rate and duty factor. This means that zoom-TOFMS could be used to examine transient events such as chromatographic peaks with both a full-spectral scan (CEA-TOFMS) mode to determine and quantify sample constituents and also with the zoom mode to examine any spectral areas of interest with both improved mass resolution and sensitivity.

High Duty-Cycle DOFMS

A limitation of batch-type mass analyzers such as TOFMS, DOFMS, or trapping instruments (i.e., ion trap, Orbitrap, FT-ICR) is that the duty cycle of mass analysis often falls well below unity (100%), i.e., some ions from a continuous initial ion beam are not extracted or analyzed. In an attempt to overcome this limited duty cycle, researchers have developed several methods, including ion storage between batch analyses and fill-time matching in TOFMS [63–68]. Importantly, DOFMS provides a unique platform to improve the duty cycle and throughput for velocity-based mass spectrometry. In DOFMS, all ions fly though the instrument and mass-separate over the same amount of time and then are detected across space; as a result, multiple groups (batches) of ions can fly through (and be *m*/*z*-separated in) the instrument concurrently. In a typical DOFMS experiment, ions are pushed out of the acceleration region, fly through the field-free and ion-mirror

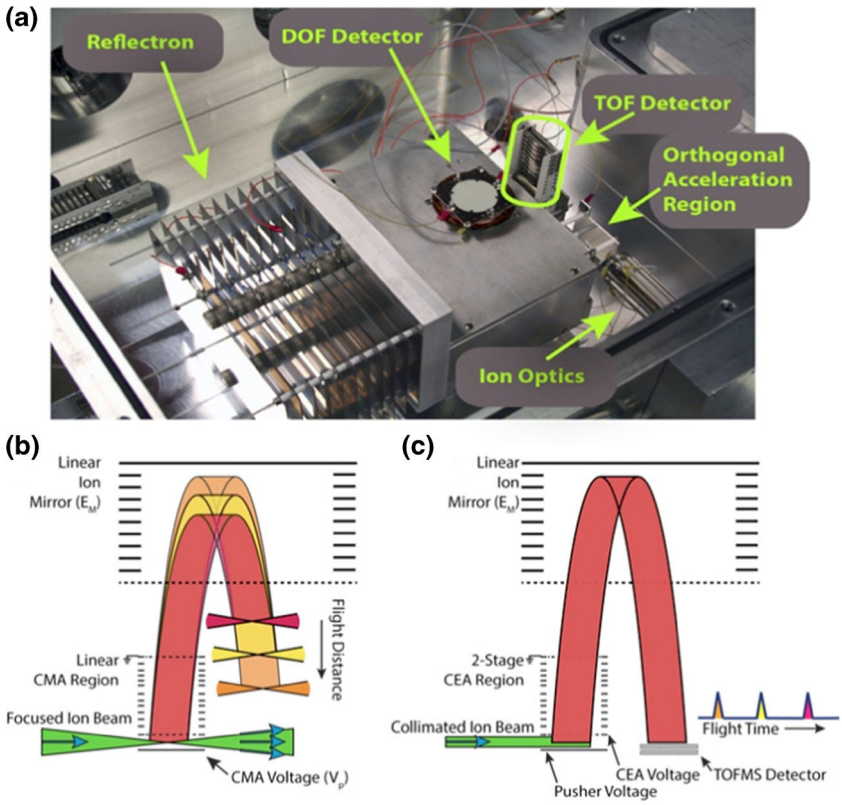

Figure 8. (**a**) Image of the first-generation DOF/TOF-MS instrument. (**b**) Schematic of DOFMS operation. In DOFMS, optimal performance is obtained if the ion beam is focused to a narrow ribbon in the acceleration region; this narrow spatial distribution is duplicated at the *m*/*z*-dependent flight distances to give high resolution for DOFMS. (**c**) Schematic of TOFMS operation. For conventional orthogonal-acceleration TOFMS, the input ion beam must be collimated and a two-stage acceleration region is used to space-focus ions at the focal point of the reflectron in order to optimize resolution [40]

regions, and then are all directed onto the detector, so the detector actually sits idle most of the time. By interleaving DOF experiments (extraction events), two or more batches of ions can be mass-separated within a single DOFMS flight time. In turn, this operation increases the duty cycle and the measured ion flux proportionally [42]. Interleaved DOFMS requires no modifications to hardware, just a new ion-pulsing scheme. Figure 7 demonstrates the improvement in detected ion signal for the interleaved MS approach, in which two ion packets were in flight at the same time.

The first results of interleaved DOFMS demonstrate a 2-fold duty-factor enhancement, and twice the sensitivity of conventional DOFMS. Future implementations of interleaved DOFMS will aim to improve the duty cycle to unity (100%), and thus match the ion throughput of continuous MS analyzers such as QMS and SFMS, but for a single *m*/*z* or a range of *m*/*z* values, respectively, measured across the DOFMS detector array. This improvement in duty cycle would be achieved with the use of the same method utilized to achieve 59% duty cycle for zoom-TOFMS [48]. In this way, interleaved DOFMS could prove especially useful for high-sensitivity isotope-ratio measurements or other applications that demand high throughput. Moreover, the mass range available for interleaved DOFMS depends only on the length of the DOFMS detector. There is a tradeoff between detector length and the duty cycle available with interleaved DOFMS because, with a very long detection system, low-*m*/*z* ions from subsequent DOF pulses could be present in the DOF detection region at the t_{ef} of a preceding experiment. However, these spectral overlaps can be easily identified, and with a longer detector, each injected ion pulse will cover a broader mass range, so duty-cycle enhancement is less critical.

Combined DOF/TOF-MS

A clear limitation of DOFMS is its inability to analyze a wide range of *m*/*z*-values for each acceleration event, due to finite detector dimensions. There are several ways to improve mass-spectral coverage in DOFMS. First, a long ion-detection device can be used, but the fabrication of an overly long array of detector elements is impractical. Second, the field-free flight length can be shortened to reduce unit-mass spacing, but this approach will impair mass resolution. Third, different mass ranges can be scanned across the DOFMS detector in separate, sequential experiments. Fourth, mass-range acquisitions can be interleaved such that more than one *m*/*z*-range enters the DOFMS detection region (and is in focus) for each acquisition event—thus multiplexing the detection process. A fifth alternative is to combine DOFMS and TOFMS into a single instrument platform, to yield a new instrument concept labeled DOF/TOF-MS. In this concept, TOFMS functions as the whole-spectrum mass analyzer, while DOFMS is used over only critical mass windows in which the benefits of spatial dispersion and/or solid-state ion detection offer better performance

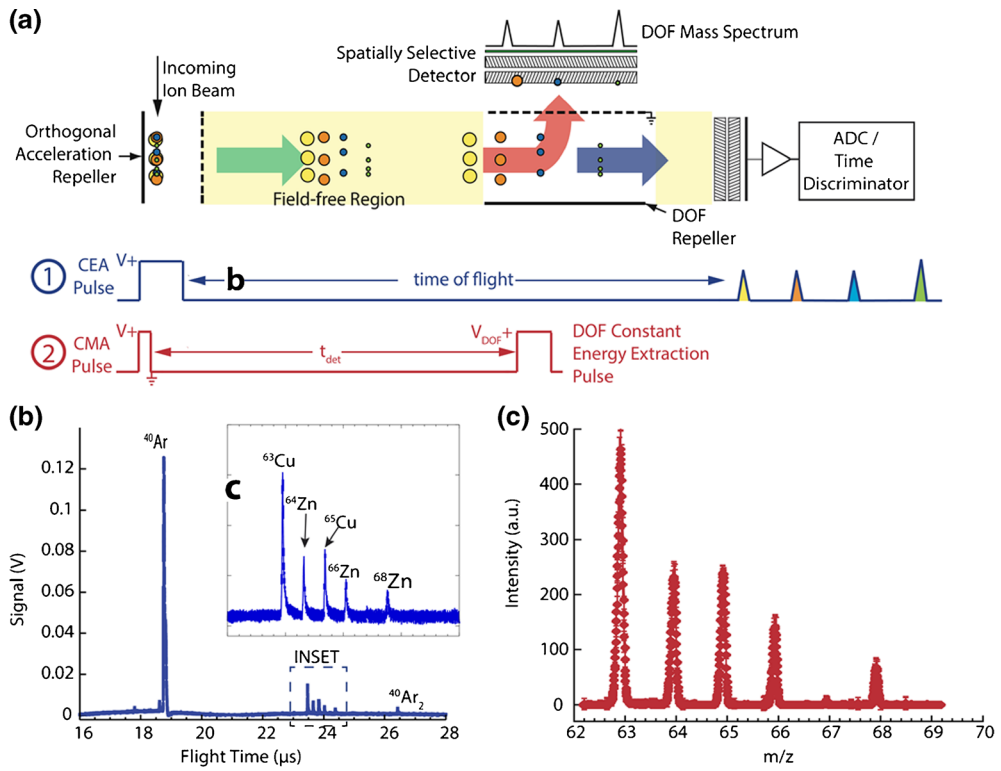

Figure 9. (**a**) Conceptual drawing and timing diagram of DOF/TOF-MS operation. (**b**) In the first step of DOF/TOF-MS a complete spectrum is collected by conventional CEA-TOFMS. (**c**) Once a region of interest is identified, this region is analyzed by DOFMS. The DOFMS spectrum presented here is a line profile from a MCP-phosphor DOFMS image [40]

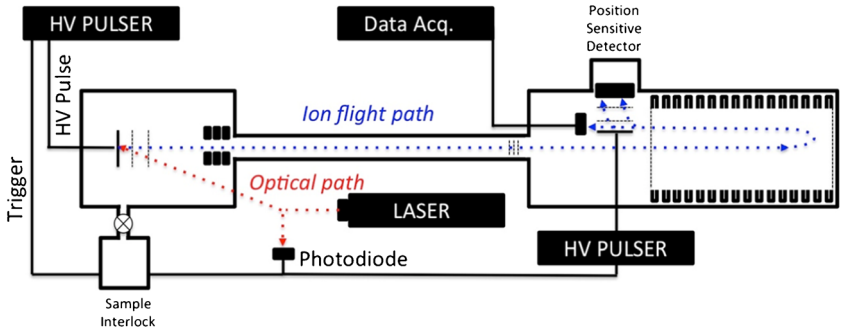

Figure 10. Schematic of a MALDI-DOFMS instrument that is also set up for DOF/TOF-MS operation. The sample plate is to the left of the diagram and the linear-field reflectron is to the right. Ions can be detected in this system either by DOFMS (pushed sideways onto the position-sensitive detector) or by TOFMS (ions pass through the DOFMS detection region and impact the stationary TOFMS detector)

than TOFMS. Here, a brief description of a hybrid DOF/TOF-MS instrument is given to illustrate the concept; more details can be found elsewhere [40, 69].

In this DOF/TOF-MS instrument, a temporally resolving detector is positioned at the end of the flight path, after the DOF detection region; this construction is fairly straightforward because DOFMS and TOFMS instruments share similar architectures (cf. Figure 2). Figure 8 provides an image of the DOF/TOF-MS instrument constructed at Indiana University and Figure 9 provides the first experimental results. The DOF/TOF-MS operational sequence is as follows: first, conventional TOFMS operation of the instrument collects a complete "reconnaissance" spectrum, from which *m/z* values that might benefit from the specialized detection capabilities of DOFMS are identified. Next, the identified *m/z*-range of interest is analyzed with DOFMS by adjusting electrostatic conditions to bring the ions into focus onto the DOFMS detector. DOF/TOF-MS might be especially valuable for the combination of chromatographic separations with DOFMS. In this case, TOFMS can be used to quickly identify the *m/z* values of eluting compounds and then interleaved DOFMS detection can be used to provide high-throughput, high-dynamic range detection of the compounds in a data-dependent manner.

Very High Mass MALDI-DOFMS

One particularly interesting area for future application of DOFMS is matrix-assisted laser desorption ionization

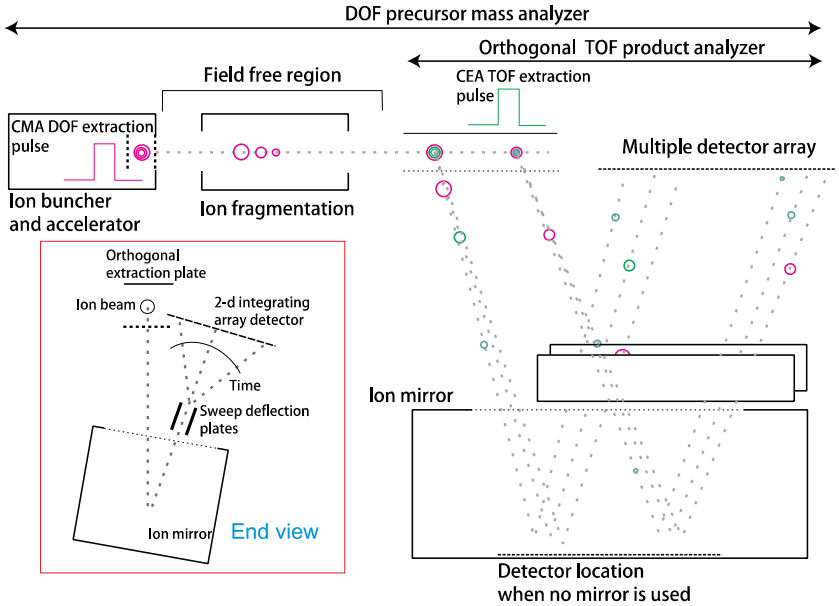

Figure 11. Illustration of a hypothetical (but realizable) instrument that could detect product ions from multiple precursor masses without losing precursor-mass information. It employs a DOFMS configuration with CMA, linear reflectron, and timed orthogonal acceleration to the detector. Precursor ions are fragmented on-the-fly by prompt dissociation, perhaps by photons or on-the-fly electron capture. Product ions retain the velocity of their precursor. In the TOFMS section, the orthogonal flight path to the detector is long enough to produce an ion-arrival time that is dependent on the product ion *m/z*. As in DOFMS, the arrival position is related to the precursor *m/z*

(MALDI), or other surface-based ionization techniques such as surface-assisted laser-desorption ionization (SALDI) or laser-induced acoustic desorption (LIAD). Because these approaches physically restrict ionization to a surface, ions are created in a relatively confined spatial region and therefore form a narrow initial ion-packet size. This inherently narrow ion packet provides a significant advantage in DOFMS, as the initial ion-packet width limits the best possible mass resolution. Coupling DOFMS with MALDI, or other pulsed ionization schemes, is also inherently efficient. A schematic of the MALDI-DOFMS instrument fabricated at Indiana University, but not yet described in the literature, is shown in Figure 10.

Use of DOFMS for the analysis of ions of high molecular weight, ranging from 1MDa to beyond 1GDa, would leverage the advantages that MS holds over more conventional biochemical approaches for the characterization of complete biological constructs. Here, DOFMS provides three critical advantages. First, like TOFMS, DOFMS relies on a simple velocity-based mass-separation strategy that has no upper-mass limit. Thus, massive ions can be separated from each other without requiring that they possess a large number of charges. For comparison, high-mass FTICR and QIT analyses typically use ESI to create ions with multiple charges, reducing the m/z of the resulting ion and increasing the effective mass range of the analyzer. Second, DOFMS employs semiconductor array detectors, like the FPC or IonCCD camera, which also possess no upper-mass limit for ion detection and that operate with no mass bias. Finally, the physical separation of ions according to m/z opens the way to expanding the utility of mass spectrometry by employing simultaneous, multi-mass soft-landing technologies.

Simultaneous MS/MS

Another extension of the distance-of-flight concept is, perhaps not surprisingly, in tandem mass spectrometry (MS/MS). What might not be expected is that the combination of DOF and TOF could, in principle, provide a means to detect all the products of multiple precursors from a single ion-extraction event. Such an instrument has yet to be built, but Figure 11 shows how it could be implemented. Just as in DOFMS, a batch of ions is extracted by CMA, but upon leaving the focusing reflectron (not shown) they undergo prompt, non-collisional fragmentation. This prompt (submicrosecond time scale) dissociation could be accomplished by high-energy photon excitation or electron-capture dissociation on-the-fly. A characteristic of dissociation produced by internal excitation rather than energetic collision with a molecule is that the ionic and neutral products both maintain the precursor's velocity. (The recoil effect from the release of the broken bond's energy will cause a small variation.) Following dissociation, the product ion's axial position along the flight path is dependent on its *precursor ion's* m/z. Now the *product ion's* m/z can be determined by orthogonal TOFMS. In other words, the product ions will be constant-energy accelerated into a TOFMS system instead of directly to a DOFMS detector. At the end of the TOFMS flight path is positioned an array of detectors that can determine each ion's arrival time (related to product m/z) and its position (related to precursor m/z). The detector could be an array of time-resolved detectors or, using the sweep arrangement shown in the *End view* inset, a 2-D detector array as used in image detection. Such an instrument could provide all the information available with the Q-TOF configuration but for a range of precursor masses on each acceleration event.

The development of such an instrument would present a number of challenges, but could be just one step beyond the development of a commercially available DOFMS instrument. The prospect of achieving a full map of product ions for a range of precursor masses on each acceleration pulse could further expand the practical applications of MS/MS.

Conclusion

The emerging, expanding, and evolving DOFMS approach opens up a new island of possibilities in the mass spectrometry landscape. The technique's ability to energy-focus ions and spatially separate m/z-values without the use of magnets or cyclotron frequencies is unprecedented in the field. A broad range of applications can be envisioned and will likely expand in the future.

Acknowledgments

This study was supported in part by the U.S. Department of Energy through grant DE-FG02-98ER14890. Early studies in DOFMS were performed in collaboration with David W. Koppenaal and Charles J. Barinaga and supported in part by Pacific Northwest National Laboratory, operated for the U.S. DOE by Battelle Memorial Institute under Contract DE-AC06-76RLO-1830op.

References

1. Zapata, F., de la Ossa Fernández, M.Á., García-Ruiz, C.: Emerging spectrometric techniques for the forensic analysis of body fluids. TrAC Trends Anal. Chem. **64**(0), 53–63 (2015)
2. Hoffmann, W.D., Jackson, G.P.: Forensic Mass Spectrometry. Annu. Rev. Anal. Chem. **8**(1), 419–440 (2015)
3. Gibbon, R.J., Granger, D.E., Kuman, K., Partridge, T.C.: Early Acheulean technology in the Rietputs Formation, South Africa, dated with cosmogenic nuclides. J. Human Evol. **56**(2), 152–160 (2009)
4. Fedosseev, V.N., Yu, K., Mishin, V.I.L.: Resonance laser ionization of atoms for nuclear physics. Phys. Scr. **85**(5), 058104 (2012)
5. Sephton, M.A.: Pyrolysis and mass spectrometry studies of meteoritic organic matter. Mass Spectrom. Rev. **31**(5), 560–569 (2012)
6. Strashnov, I., Gilmour, J.D.: Resonance ionisation mass spectrometry of krypton and its applications in planetary science. Hyperfine Interact. **227**(1/3), 259–270 (2014)
7. Palmer, P.T., Limero, T.F.: Mass spectrometry in the U.S. space program: past, present, and future. J. Am. Soc. Mass. Spectrom. **12**, 656–675 (2001)
8. Kylander-Clark, A.R.C., Hacker, B.R., Cottle, J.M.: Laser-ablation split-stream ICP petrochronology. Chem. Geol. **345**, 99–112 (2013)
9. Hewitt, C.N., Hayward, S., Tani, A.: The application of proton transfer reaction-mass spectrometry (PTR-MS) to the monitoring and analysis of volatile organic compounds in the atmosphere. J. Environ. Monit. **5**(1), 1–7 (2003)
10. Pratt, K.A., Prather, K.A.: Mass spectrometry of atmospheric aerosols—recent developments and applications Part I: Off-line mass spectrometry techniques. Mass Spectrom. Rev. **31**(1), 1–6 (2012)

11. Brandt, J., Oehlenschlaeger, K.K., Schmidt, F.G., Bamer-Kowollik, C., Lederer, A.: State-of-the-art analytical methods for assessing dynamic bonding soft matter materials. Adv. Mater. **26**(33), 5758–5785 (2014)
12. Buchberger, A., Yu, Q., Li, L.: Advances in mass spectrometric tools for probing neuropeptides. Annu. Rev. Anal. Chem. **8**(1), 485–509 (2015)
13. Yuan, Z.-F., Arnaudo, A.M., Garcia, B.A.: Mass spectrometric analysis of histone proteoforms. Annu. Rev. Anal. Chem. **7**(1), 113–128 (2014)
14. Rodríguez-Suárez, E., Whetton, A.D.: The application of quantification techniques in proteomics for biomedical research. Mass Spectrom. Rev. **32**(1), 1–26 (2013)
15. Marshall, A.G., Hendrickson, C.L.: High-resolution mass spectrometers. Annu. Rev. Anal. Chem. **1**(1), 579–599 (2008)
16. Jakubowski, N., Prohaska, T., Vanhaecke, F., Roos, P.H., Lindemann, T.: Inductively coupled plasma- and glow discharge plasma-sector field mass spectrometry Part II. Applications. J. Anal. Atomic Spectrom. **26**(4), 727–757 (2011)
17. Enke, C.G.: The unique capabilities of time-of-flight mass analyzers. In: Advances in mass spectrometry, Vol. 14, pp. 197–219. Elsevier Science Publishers B.V.: Amsterdam (1998)
18. Hammer, W.: Zeitschrift fur Physik **12**, 1077 (1911)
19. Thomson, J.J.: Rays of positive electricity. Proc. Royal Soc. London **89**(A), 1–20 (1913)
20. Smith, L.G.: A new magnetic period mass spectrometer. Rev. Sci. Instrum. **22**(2), 115–116 (1951)
21. Sommer, H., Thomas, H.A., Hipple, J.A.: Measurement of E/M by cyclotron resonance. Phy. Rev. **82**, 697–702 (1951)
22. Paul, W., Raether, M.: Das elektrische Massenfilter. Zeitschrift fur Physik **140**, 262–273 (1955)
23. Paul, W., Steinwedel, H.: A new mass spectrometer without magnetic field. Zeitschrift fur Naturforschung **8A**, 448–450 (1953)
24. Yost, R.A., Enke, C.G.: Selected ion fragmentation with a tandem quadrupole mass spectrometer. J. Am. Chem. Soc. **100**, 2274–2275 (1978)
25. Yost, R.A., Enke, C.G., McGilvery, D.C., Smith, D., Morrison, J.D.: High efficiency collision-induced dissociation in an rf-only quadrupole. Int. J. Mass Spectrom. **30**, 27–136 (1979)
26. Yost, R.A., Enke, C.G.: Triple quadrupole mass spectrometry for direct mixture analysis and structure eluciation. Anal. Chem. **51**, 1251A–1262A (1979)
27. McGilvery, D.C., Morrison, J.D.: A mass spectrometer for the study of laser-induced photodissociation of ions. Int. J. Mass Spectrom. **28**(1), 81–92 (1978)
28. Makarov, A.: Electrostatic axially harmonic orbital trapping: a high-performance technique of mass analysis. Anal. Chem. **72**(6), 1156–1162 (2000)
29. Enke, C.G., Dobson, G.S.: Achievement of energy focus for distance-of-flight mass spectrometry with constant momentum acceleration and an ion mirror. Anal. Chem. **79**, 8650–8661 (2007)
30. McLuckey, S.A., Wells, J.M.: Mass analysis at the advent of the 21st century. Chem. Rev. **101**(2), 571–606 (2001)
31. Brunnée, C.: The ideal mass analyzer: Fact or fiction? Int. J. Mass Spectrom. Ion Processes **76**(2), 125–237 (1987)
32. Gross, J.H.: Mass spectrometry: a textbook. Springer-Verlag, Berlin (2004)
33. Radionova, A., Filippov, I., Derrick, P.J.: In pursuit of resolution in time-of-flight mass spectrometry: a historical perspective. Mass Spectrom. Rev. (2015). doi:10.1002/mas.21470.
34. Dennis, E.A., Gundlach-Graham, A.W., Enke, C.G., Ray, S.J., Carado, A.J., Barinaga, C.J., Koppenaal, D.W., Hieftje, G.M.: How constant momentum acceleration decouples energy and space focusing in distance-of-flight and time-of-flight mass spectrometries. J. Am. Soc. Mass Spectrom. **24**(5), 690–700 (2013)
35. Wiley, W.C., McLaren, I.H.: Time-of-flight mass spectrometer with improved resolution. Rev. Sci. Instrum. **26**(12), 1150–1157 (1955)
36. Wolff, M.M., Stephens, W.E.: A pulsed mass spectrometer with time dispersion. Rev. Sci. Instrum. **24**(8), 616–617 (1953)
37. Cotter, R.J.: Time-of-flight mass spectrometry, Vol. **549**. Am. Chem. Soc. Washington DC (1994).
38. Dennis, E., Ray, S., Gundlach-Graham, A., Enke, C., Barinaga, C., Koppenaal, D.: Hieftje, G.:Constant-momentum acceleration time-of-flight mass spectrometry with energy focusing. J. Am. Soc. Mass Spectrom. **24**(12), 1853–1861 (2013)
39. Graham, A.W.G., Ray, S.J., Enke, C.G., Barinaga, C.J., Koppenaal, D.W., Hieftje, G.M.: First distance-of-flight instrument: opening a new paradigm in mass spectrometry. J. Am. Soc. Mass Spectrom. **22**, 110–117 (2011)
40. Gundlach-Graham, A.W.: Distance-of-flight mass spectrometry: theory, instrumentation, and practice. Indiana University (2013).
41. Graham, A.W.G., Ray, S.J., Enke, C.G., Felton, J.A., Carado, A.J., Barinaga, C.J., Koppenaal, D.W., Hieftje, G.M.: Resolution and mass range performance in distance-of-flight mass spectrometry with a multi-channel focal-plane camera detector. Anal. Chem. **83**(22), 8552–8559 (2011)
42. Gundlach-Graham, A., Dennis, E., Ray, S., Enke, C., Barinaga, C., Koppenaal, D., Hieftje, G.: Interleaved distance-of-flight mass spectrometry: a simple method to improve the instrument duty factor. J. Am. Soc. Mass Spectrom. **24**(11), 1736–1744 (2013)
43. Gundlach-Graham, A.W., Dennis, E.A., Ray, S.J., Enke, C.G., Carado, A.J., Barinaga, C.J., Koppenaal, D.W., Hieftje, G.M.: Extension of the focusable mass range in distance-of-flight mass spectrometry with multiple detectors. Rapid Commun. Mass Spectrom. **26**(21), 2526–2534 (2012)
44. Gundlach-Graham, A., Dennis, E.A., Ray, S.J., Enke, C.G., Barinaga, C.J., Koppenaal, D.W., Hieftje, G.M.: First inductively coupled plasma-distance-of-flight mass spectrometer: instrument performance with a microchannel plate/phosphor imaging detector. J. Anal. At. Spectrom. **28**(9), 1385–1395 (2013)
45. Dennis, E.A., Ray, S.J., Enke, C.G., Gundlach-Graham, A.W., Barinaga, C.J., Koppenaal, D.W., Hieftje, G.M.: Distance-of-flight mass spectrometry with IonCCD detection and an inductively coupled plasma source. J. Am. Soc. Mass Spectrom. **27**(3), 371–379 (2016)
46. Gundlach-Graham, A., Dennis, E.A., Ray, S.J., Enke, C.G., Barinaga, C.J., Koppenaal, D.W., Hieftje, G.M.: Laser-ablation sampling for inductively coupled plasma distance-of-flight mass spectrometry. J. Anal. At. Spectrom. **30**(1), 139–147 (2015)
47. Guilhaus, M.: Special feature: Tutorial. Principles and instrumentation in time-of-flight mass spectrometry. Physical and instrumental concepts. J. Mass Spectrom. **30**(11), 1519–1532 (1995)
48. Dennis, E.A., Gundlach-Graham, A.W., Ray, S.J., Enke, C.G., Barinaga, C.J., Koppenaal, D.W., Hieftje, G.M.: Zoom-TOFMS: addition of a constant-momentum-acceleration "zoom" mode to time-of-flight mass spectrometry. Anal. Bioanal. Chem. **406**(29), 7419–7430 (2014)
49. Gilmore, I.S., Seah, M.P.: Ion detection efficiency in SIMS: Dependencies on energy, mass, and composition for microchannel plates used in mass spectrometry. Int. J. Mass Spectrom. **202**(1/3), 217–229 (2000)
50. Frazer, G.W.: The ion detection efficiency of microchannel plates (MCPs). Int. J. Mass Spectrom. **215**, 13–30 (2000)
51. Fraser, G.W.: The operation of microchannel plates at high count rates. Nucl. Instrum. Methods A **306**, 247–260 (1991)
52. Hadjar, O., Johnson, G., Laskin, J., Kibelka, G., Shill, S., Kuhn, K., Cameron, C., Kassan, S.: IonCCD for direct position-sensitive charged-particle detection: from electrons and kev ions to hyperthermal biomolecular ions. J. Am. Soc. Mass Spectrom. **22**(4), 612–623 (2011)
53. Cyriac, J., Wleklinski, M., Li, G., Gao, L., Cooks, R.G.: In situ Raman spectroscopy of surfaces modified by ion soft landing. Analyst (Cambridge, U K) **137**(6), 1363–1369 (2012)
54. Mikhailov, V.A., Mize, T.H., Benesch, J.L.P., Robinson, C.V.: Mass-selective soft-landing of protein assemblies with controlled landing energies. Anal. Chem. **86**(16), 8321–8328 (2014)
55. Griffin, C.E., Boettger, H.G., Norris, D.D.: An electro-optical detector for focal plane mass spectrometers. Int. J. Mass Spectrom. **15**(4), 437–449 (1974)
56. Barnes IV, J.H., Schilling, G.D., Sperline, R., Denton, M.B., Young, E.T., Barinaga, C.J., Koppenaal, D.W., Hieftje, G.M.: Characterization of a focal plane camera fitted to a Mattauch-Herzog geometry mass spectrograph. 2. Use with an inductively coupled plasma. Anal. Chem. **76**(9), 2531–2536 (2004)
57. Barnes IV, J.H., Sperline, R., Denton, M.B., Barinaga, C.J., Koppenaal, D., Young, E.T., Hieftje, G.M.: Characterization of a focal plane camera fitted to a Mattauch-Herzog geometry mass spectrograph. 1. Use with a glow-discharge source. Anal. Chem. **74**(20), 5327–5332 (2002)
58. Barnes IV, J.H., Hieftje, G.M.: Recent advances in detector-array technology for mass spectrometry. Int. J. Mass Spectrom. **238**(1), 33–46 (2004)
59. Koppenaal, D.W., Barinaga, C.J., Denton, M.B., Sperline, R.P., Hieftje, G.M., Schilling, G.D., Andrade, F.J., Barnes, J.H.I.: Mass spectrometry detectors. Anal. Chem. **77**(21), 418A–427A (2005)
60. Schilling, G., Andrade, F.J., Barnes, J.H., Sperline, R.P., Denton, M.B., Barinaga, C.J., Koppenaal, D.W., Hieftje, G.M.: Characterization of a second-generation focal-plane camera coupled to an inductively coupled plasma Mattauch-Herzog geometry mass spectrograph. Anal. Chem. **78**(13), 4319–4325 (2006)

61. Schilling, G.D., Ray, S.J., Rubinshtein, A.A., Felton, J.A., Sperline, R.P., Denton, M.B., Barinaga, C.J., Koppenaal, D.W., Hieftje, G.M.: Evaluation of a 512-channel Faraday-strip array detector coupled to an inductively coupled plasma Mattauch-Herzog mass spectrograph. Anal. Chem. **81**(13), 5467–5473 (2009)
62. Schilling, G.D., Ray, S.J., Sperline, R.P., Denton, M.B., Barinaga, C.J., Koppenaal, D.W., Hieftje, G.M.: Optimization of Ag isotope-ratio precision with a 128-channel array detector coupled to a Mattauch-Herzog mass spectrograph. J. Anal. At. Spectrom. **25**(3), 322–327 (2010)
63. Boyle, J.G., Whitehouse, C.M., Fenn, J.B., Cotter, R.J.: An ion-storage time-of-flight mass spectrometer for analysis of electrospray ions. Rapid Commun. Mass Spectrom. **5**(9), 400–405 (1991)
64. Chien, B.M., Michael, S.M., Lubman, D.M.: The design and performance of an ion trap storage reflectron time-of-flight mass spectrometer. Int. J. Mass Spectrom. Ion Processes **131**, 149–179 (1994)
65. Chambers, D.M., Grace, L.I., Andresen, B.D.: Development of an ion store/time-of-flight mass spectrometer for the analysis of volatile compounds in air. Anal. Chem. **69**(18), 3780–3790 (1997)
66. Chernushevich, I.V.: Duty cycle improvement for a quadrupole-time-of-flight mass spectrometer and its use for precursor ion scans. Eur. J. Mass Spectrom. **6**(6), 471–480 (2000)
67. Hashimoto, Y., Hasegawa, H., Satake, H., Baba, T., Waki, I.: Duty cycle enhancement of an orthogonal acceleration TOF mass spectrometer using an axially-resonant excitation linear ion trap. J. Am. Soc. Mass Spectrom. **17**(12), 1669–1674 (2006)
68. Brenton, A.G., Krastev, T., Rousell, D.J., Kennedy, M.A., Craze, A.S., Williams, C.M.: Improvement of the duty cycle of an orthogonal acceleration time-of-flight mass spectrometer using ion gates. Rapid Commun. Mass Spectrom. **21**(18), 3093–3102 (2007)
69. Enke, C.G., Ray, S.J., Graham, A.W., Hieftje, G.M., Barinaga, C.J., Koppenaal, D.W.: Combined distance-of-flight and time-of-flight mass spectrometer. US Patent 20130092832: (2013)